Journal of Materials Processing Technology 153–154 (2004) 765–770

Journal of Materials Processing Technology

www.elsevier.com/locate/jmatprotec

Direct and inverted open die extrusion (ODE) of rods and tubes

K. Srinivasan [a,*], P. Venugopal [b]

[a] Department of Metallurgical and Materials Engineering, National Institute of Technology, Surathkal, Srinivasnagar 575025, India

[b] Metal Forming Lab, Department of Metallurgical Engineering, Indian Institute of Technology, Chennai 600036, India

Abstract

Open die extrusion (ODE) has been done on AISI 1020 steel, commercial purity aluminium and commercial purity titanium, in both direct and inverted modes. It was found that inverted extrusion requires lesser forces than direct extrusion. Limit strains are more for the former than for the later as measured experimentally and as calculated theoretically. Theoretical limit strains are lesser than experimental ones in both the case of rods and tubes. ODE is only for shorter components due to unsupported billet and interference from buckling. It is also only for smaller strains due to interference from upsetting of unsupported billet above the die rather than extrusion through the die.

Keywords: Open die; Titanium; Aluminium; Steel; Direct; Inverted rod; Tube

1. Introduction

Open die extrusion (ODE) is done without container as against conventional extrusion, which is done with container [1]. Therefore, container wall–billet frictional force is eliminated in ODE. This leads to a large reduction in the total force required for extrusion. Surface quality is expected to be better due to absence of friction. As there is no container, the billet is not supported and there is the danger of buckling of billet if its height to diameter ratio is greater than 3. Therefore ODE is only for producing short components [2,3]. Moreover, if punch pressure for ODE is greater than yield stress, upsetting of billet will take place above the die rather than extrusion through the die. Therefore, only smaller strains can be imparted in a single stage (i.e., per pass) [4]. In spite of the above two limitations, this process becomes attractive due to reduced forces and better finish for product shapes shown in Fig. 1.

2. Experimental

Compression test, ring compression test and extrusion tests have been carried out on annealed AISI 1020 steel, commercial purity aluminium and commercial purity titanium.

2.1. Compression test

Two HCHCr cylindrical pieces were used as upper and lower platens, and workpieces of diameter 25 mm and height to diameter (ho/do) ratio of 1.5 were compressed using a hydraulic press of 100 T capacity. Molybdenum disulphide was used as lubricant. Using loadcell, LVDT, amplifier and x–y recorder force–stroke diagrams were recorded. From these recordings, stress and strain were determined and plotted to get yield stress (S_y). Log stress versus log strain was plotted to determine strength coefficient (K) and strain hardening exponent (n). Constitutive equations of the form $\sigma = K\varepsilon^n$ were developed.

2.2. Ring compression test

Rings of outer diameter 24 mm and outer diameter:inner diameter:initial height (OD:ID:ho) = 6:3:2 were compressed in the same press using the same platens as discussed in Section 2.1 with molybdenum disulphide as lubricant. The change in inner diameter and reduction in height were measured and using a standard chart [5] Coloumb friction coefficient was determined.

2.3. Open die extrusion tests

The experimental set up for direct open die extrusion test for rod and tube are shown in Figs. 2 and 3, respectively. Die is stationary and is resting on the bed of the 100 T hydraulic press. The billet is pushed by the press ram vertically downwards. Molybdenum disulphide was used as lubricant. Force

* Corresponding author. Tel.: +91 824 476 494; fax: +91 824 476 090.
E-mail addresses: ksrini@krec.ac.in, ksrini@nitk.ac.in (K. Srinivasan), pvenu@acer.iitm.ernet.in (P. Venugopal).

0924-0136/$ – see front matter © 2004 Elsevier B.V. All rights reserved.
doi:10.1016/j.jmatprotec.2004.04.177

Nomenclature

A	surface area of deformation zone
A_f	final area of cross section
A_0	initial area of cross section
C	specific heat
d_{iB}	inner diameter of billet
d_{oB}	outer diameter of billet
d_{iE}	inner diameter of extrude
d_{oE}	outer diameter of extrude
F	force
F_{dfr}	die friction force
F_{id}	ideal force
F_{mfr}	mandrel friction force
F_{sh}	shear force
K	strength coefficient
n	strain hardening experiment
P_P	punch pressure
S_y	yield stress
Δt	time interval of extrusion
v_R	velocity of ram
V	volume of deformation zone

Greek letters

α	semi-die angle
β	0.95
ϵ	strain
ϵ_L	limit strain
μ	Coloumb friction coefficient
σ_{fm}	mean flow stress $= K\varepsilon^n/n+1$
σ_N	stress normal to inclined face in the deformation zone of die
ρ	density

stroke diagrams were recorded. After an initial rise, force remained constant if there was pure extrusion. If upsetting interfered, force increased with increasing movement of ram and there was a discontinuity. A change in slope occurs distinguishing the initial die filling and upsetting regions.

The experimental set up for inverted open die extrusion test for rod and tube are shown in Figs. 4 and 5, respectively. These differ from direct extrusion set up. Die was attached to the press ram and was moving down during extrusion while billet was flowing upwards. The friction coefficient is expected to be less in inverted extrusion due to the above dynamic situation. Force–stroke diagrams were recorded. Experimental punch pressures were determined from forces measured and theoretical punch pressures were calculated using slab theory.

3. Results and discussion

The results of compression and ring compression tests are shown in Table 1.

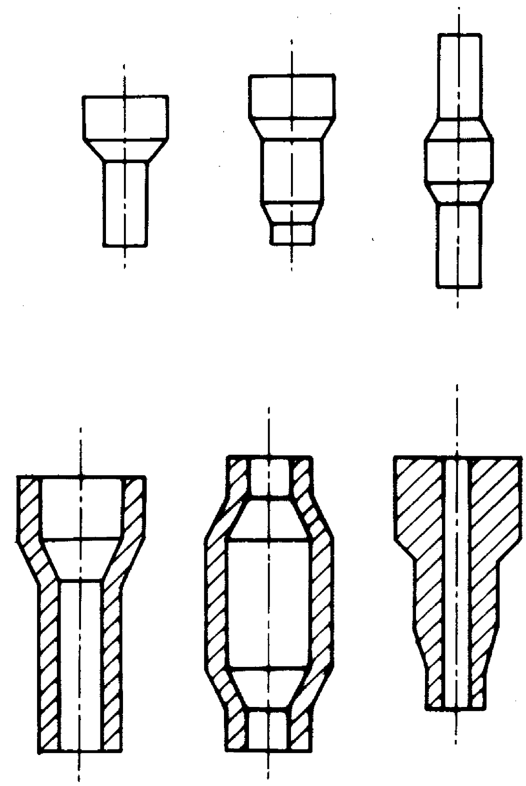

Fig. 1. Product shapes that can be produced by open die extrusion.

The results of open die extrusion are shown in Figs. 6–9 for direct rod, inverted rod, direct tube and inverted tube cases, respectively. For rod the die angle is 25° and for tube the die angle is 30°. These were found to be the optimum

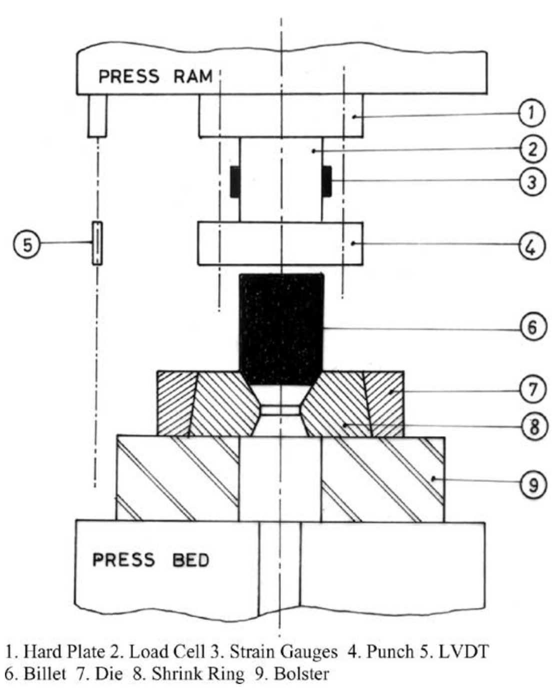

Fig. 2. Experimental set up for direct rod ODE.

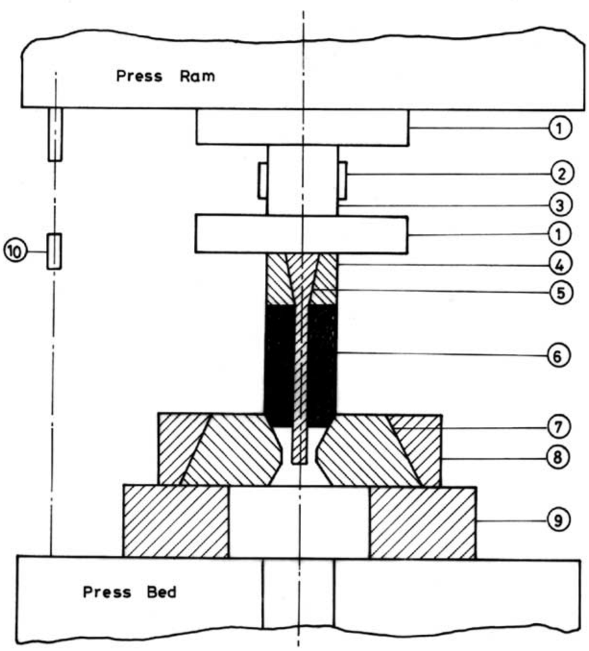

1. Hard Plate 2. Strain Gauge 3. Load Cell 4. Sleeve
5. Mandrel 6. Hollow Billet 7. Die Ring 8. Shrink Ring
9. Bolster 10. LVDT

Fig. 3. Experimental set up for direct tube ODE.

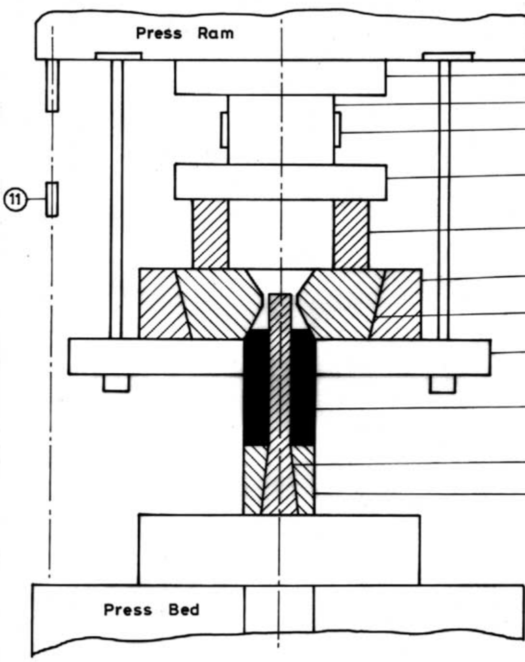

1. Head Plate 2. Load Cell 3. Strain Gauge 4. Bolster
5. Shrink Ring 6. Die Ring 7. Support for Die 8. Hollow Billet
9. Mandrel 10. Sleeve 11. LVDT

Fig. 5. Experimental set up for inverted tube ODE.

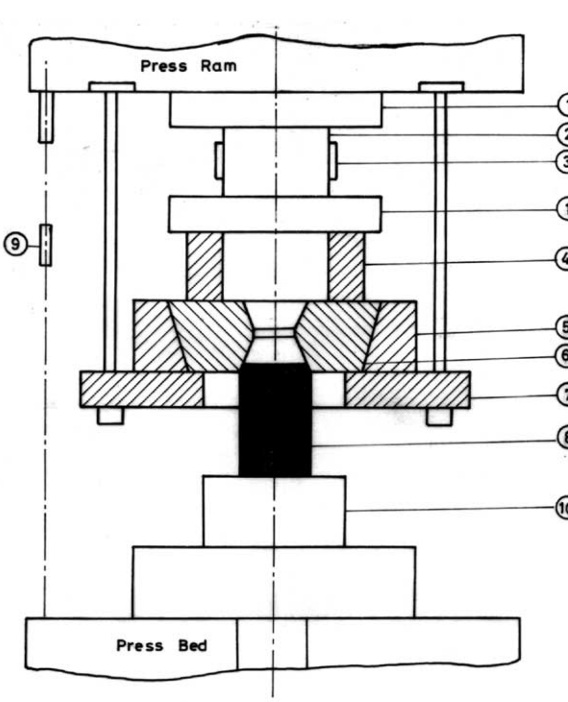

1. Hard Plate 2. Load Cell 3. Strain Gauge 4. Bolster
5. Shrink Ring 6. Die Ring 7. Support for Die 8. Billet 9. LVDT
10. Punch

Fig. 4. Experimental set up for inverted rod ODE.

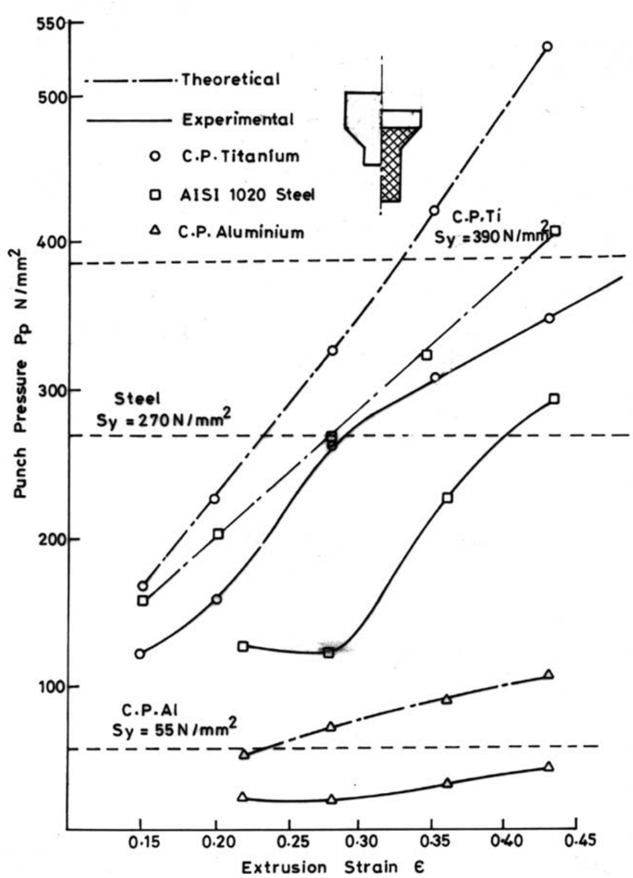

Fig. 6. Variation of punch pressure with extrusion strain for direct rod ODE.

Table 1
Flow properties

Material	K (MPa)	n	μ	S_y (MPa)
AISI 1020 steel	815	0.27	0.10	270
Commercial purity aluminium	180	0.21	0.14	55
Commercial purity titanium	1100	0.34	0.14	390

angles as has been reported elsewhere [6]. Variation of individual force components with die angle in rod and tube ODE are shown in Figs. 10 and 11 schematically. As extrusion strain increases punch pressure increases. Theoretical punch pressures are more than experimental punch pressures due to temperature rises in the deformation zone during extrusion. It has been measured by placing a thermocouple in the extrude at the middle of the exit face at the bottom. It was found to go up to 85 °C in the case of titanium. The discrepancy in the theoretical and experimental punch pressures is attributed to this factor. When the punch pressure for extrusion equals the yield stress for a particular extrusion strain, that strain is called the limit strain. If punch pressure exceeds yield stress upsetting of billet above the die will dominate rather than extrusion of billet through the die. Therefore limit strain is the maximum possible strain in

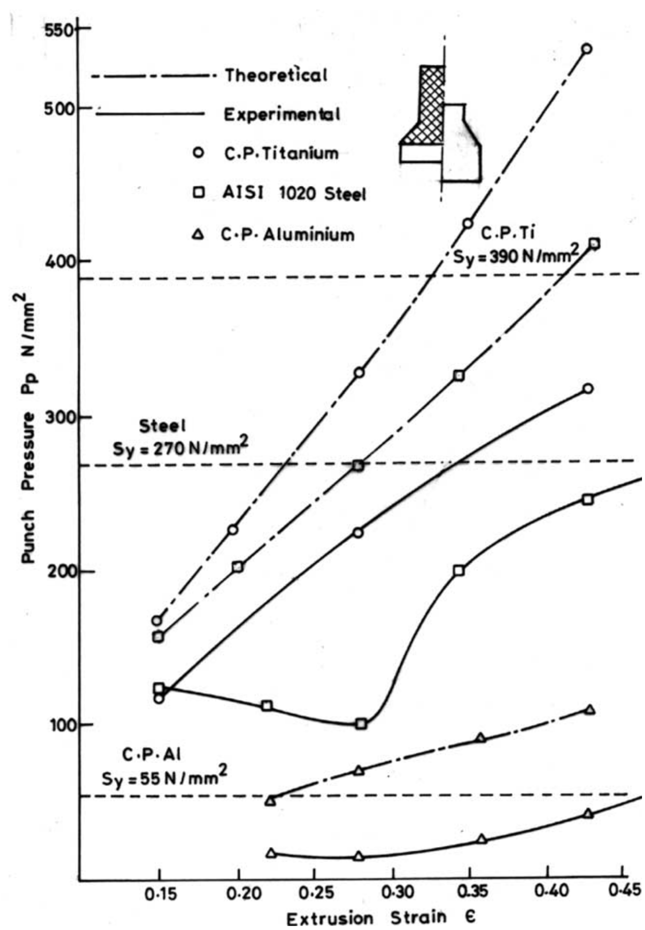

Fig. 7. Variation of punch pressure with extrusion for inverted rod ODE.

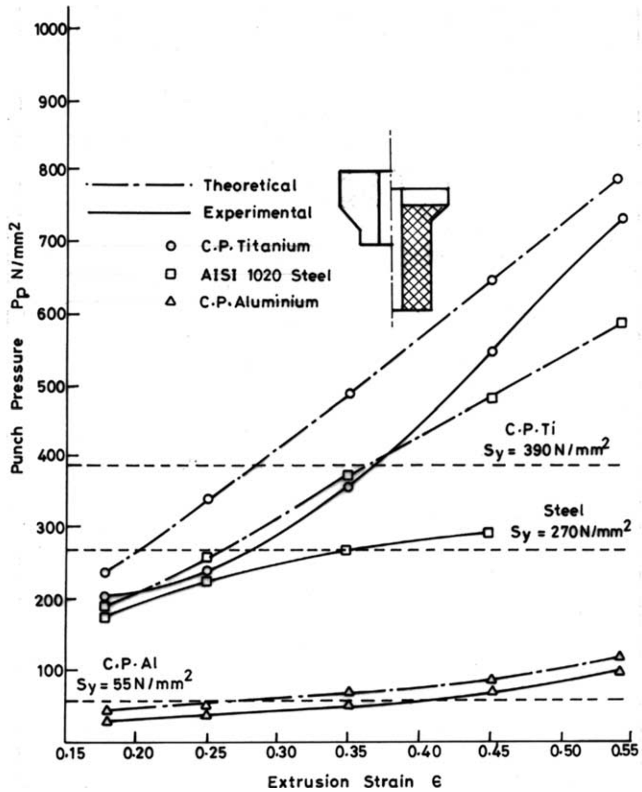

Fig. 8. Variation of punch pressure with extrusion strain for direct tube ODE.

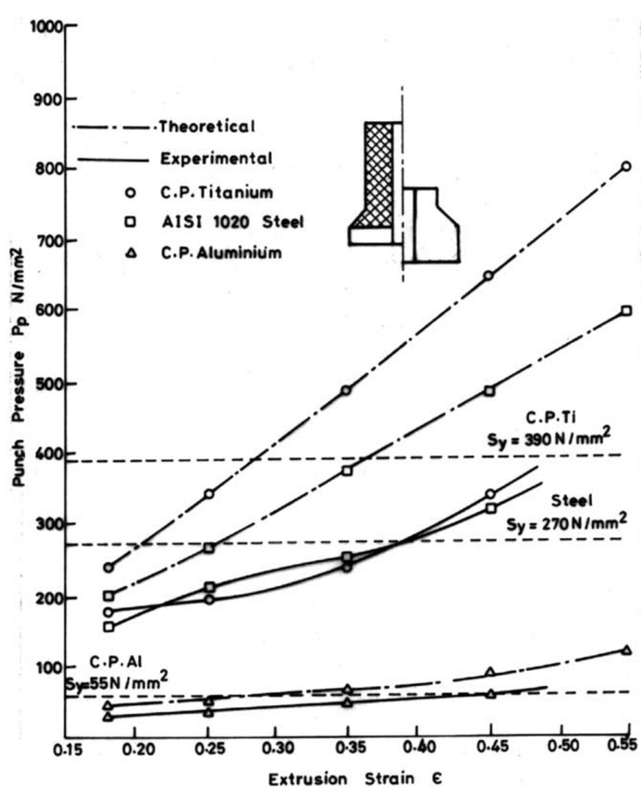

Fig. 9. Variation of punch pressure with extrusion strain for inverted tube ODE.

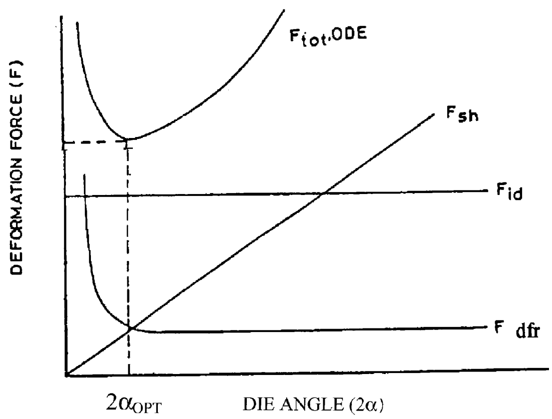

Fig. 10. Variation of individual force components with die angle for rod ODE at a given extrusion strain (schematic).

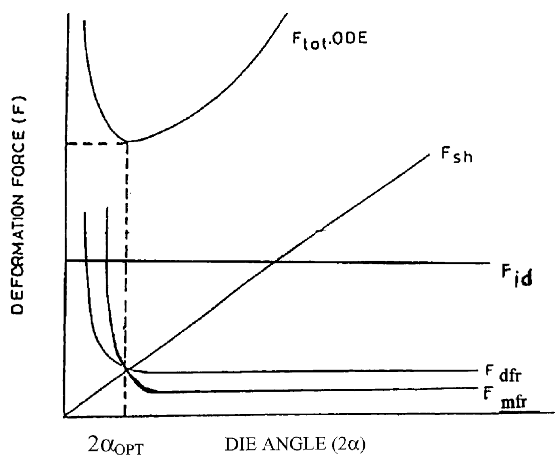

Fig. 11. Variation of individual force components with die angle for tube ODE at a given extrusion strain (schematic).

one pass for carrying out pure open die extrusion. The limit strains for various cases are given in Table 2.

From this table following results are evident: (i) theoretical limit strains are less than experimental limit strains in all cases; (ii) limit strains for rod are more than that of tube; (iii) limit strains for inverted open die extrusion are more than that for direct open die extrusion. The reason for the first result is temperature rise in the deformation zone. The second result is due to additional mandrel friction force. The third result is due to the dynamic situation that exists during inverted extrusion, i.e., die is moving in one direction (downwards) and billet is flowing in opposite direction (upwards) in the inverted case while the die is stationary in the direct case. Due to this die frictional force is less in the former than in the later.

4. Conclusion

Inverted open die extrusion requires lesser forces compared with direct open die extrusion. Limit strains are more for the former than for the later. Shorter components can be produced with good quality. Consumption of lubricant is less. Tooling required is less complex compared with conventional extrusion.

Appendix A. Individual force components in ODE [7,8]

Component	Rod	Tube
Ideal force	$A_0\varepsilon\sigma_{\mathrm{fm}}$	$A_0\varepsilon\sigma_{\mathrm{fm}}$
Shear force	$A_0(2\alpha/3)\sigma_{\mathrm{fm}}$	$A_0(\alpha/2)\sigma_{\mathrm{fm}}$
Die friction force	$A_0(2\mu/\sin 2\alpha)\varepsilon\sigma_{\mathrm{fm}}$	$A_0(2\mu/\sin 2\alpha)\varepsilon\sigma_{\mathrm{fm}}$
Mandrel friction force	–	$A_{\mathrm{f}}(\mu/\tan\alpha)\varepsilon\sigma_{\mathrm{fm}}$

Appendix B. Formulas used in calculation [7,8]

$$\sigma = K\varepsilon^n$$

$$\sigma_{\mathrm{fm}} = \left(\frac{K(\varepsilon)^n}{n+1}\right)$$

$$\varepsilon_{\mathrm{rod}} = \ln\frac{A_0}{A_{\mathrm{f}}} = 2\ln\frac{d_0}{d_{\mathrm{f}}}$$

$$\varepsilon_{\mathrm{tube}} = \ln\frac{A_0}{A_{\mathrm{f}}} = \ln\left[\frac{d_{\mathrm{oB}}^2 - d_{\mathrm{iB}}^2}{d_{\mathrm{oE}}^2 - d_{\mathrm{iE}}^2}\right]$$

$$\text{Since } d_{\mathrm{iB}} = d_{\mathrm{iE}} = 10\,\mathrm{mm},\quad \varepsilon_{\mathrm{tube}} = \ln\left[\frac{d_{\mathrm{oB}}^2 - 10^2}{d_{\mathrm{oE}}^2 - 10^2}\right]$$

Table 2
Limit strains

Material	Process	Limit strains, ε_{L}			
		Rod		Tube	
		Theory	Experimental	Theory	Experimental
AISI 1020 steel	Direct	0.28	0.40	0.26	0.35
	Inverted	0.28	0.50	0.26	0.38
CP aluminium	Direct	0.30	0.47	0.25	0.40
	Inverted	0.30	0.49	0.25	0.45
CP titanium	Direct	0.33	0.50	0.28	0.38
	Inverted	0.33	0.55	0.28	0.48

Theoretical punch pressure:

$$P_{\mathrm{P_{rod}}} = \sigma_{\mathrm{fm}}\left[\frac{2\alpha}{3} + \varepsilon\left(1 + \frac{2\mu}{\sin 2\alpha}\right)\right]$$

$$P_{\mathrm{P_{tube}}} = \sigma_{\mathrm{fm}}\left[\frac{\alpha}{2} + \varepsilon\left(1 + \frac{2\mu}{\sin 2\alpha} + \left(\frac{A_{\mathrm{f}}}{A_0}\right)\left(\frac{\mu}{\tan\alpha}\right)\right)\right]$$

Experimental punch pressure:

$$P_{\mathrm{P_{rod}}} = \frac{F}{A_0}, \quad A_0 = \frac{\pi d_0^2}{4}$$

$$P_{\mathrm{P_{tube}}} = \frac{F}{A_0}, \quad A_0 = \frac{\pi(d_{0\mathrm{B}}^2 - 10^2)}{4}$$

Theoretical limit strain:

$$\varepsilon_{\mathrm{L_{rod}}} = \frac{(S_{\mathrm{y}}/\sigma_{\mathrm{fm}}) - (2\alpha/3)}{1 + (2\mu/\sin 2\alpha)}$$

$$\varepsilon_{\mathrm{L_{tube}}} = \frac{(S_{\mathrm{y}}/\sigma_{\mathrm{fm}}) - (\alpha/2)}{1 + (2\mu/\sin 2\alpha) + (A_{\mathrm{f}}/A_0)(\mu/\tan\alpha)}$$

Appendix C. Temperature rise in deformation zone [9,10]

$$\Delta T_{\mathrm{adiabatic}} = \frac{\beta\sigma_{\mathrm{fm}}\varepsilon}{\rho c}$$

$$\Delta T_{\mathrm{die\,friction}} = \frac{\mu\sigma_{\mathrm{N}} V_{\mathrm{R}} \cos\alpha\,\Delta t A}{\rho C V}$$

$$\Delta T_{\mathrm{sheer}} = \frac{\sigma_{\mathrm{fm}}\alpha}{2\rho C V}$$

References

[1] B. Avitzur, Handbook of Metal Forming Processes, Wiley, New York, 1983, pp. 150–151.
[2] K. Srinivasan, P. Venugopal, Warm open die extrusion of Ti–6A1–4V, J. Mater. Process. Technol. 38 (1993) 265–278.
[3] K. Srinivasan, P. Venugopal, Hardness–stress–strain correlation in titanium open die extrusion—an alternative to viscoplasticity, J. Mater. Process. Technol. 95 (1998) 185–190.
[4] K. Lange, Handbook of Metal Forming, McGraw-Hill, New York, 1985, Chapter 15, pp. 20–23.
[5] T. Altan, S. Oh, H. Gegel, Metal Forming, ASM, Ohio, 1995, Chapter 6, pp. 83–88.
[6] K. Srinivasan, P. Venugopal, Adiabatic and friction heating in the open die extrusion of solid and hollow bodies, J. Mater. Process. Technol. 70 (1997) 170–177.
[7] H. Binder, K. Lange, Investigations on Open Die Extrusion of Solid Cylindrical Workpieces, Springer-Verlag, Berlin, 1980 (in German).
[8] K. Haarschiedt, K. Lange, Investigations on Open Die Extrusion of Thickwalled Hollow Cylindried Workpiece, Springer-Verlag, Berlin, 1983 (in German).
[9] G.E. Dieter, D. Bacon, Mechanical Metallurgy, McGraw-Hill, London, 1988, pp. 524–526.
[10] K. Laue, H. Stenger, Extrusion—Processes, Machinery Tooling, ASM, Ohio, 1981, pp. 31–33.